3.3.1. General structure

Modeling of POP transport requires the physical-chemical properties of considered POPs, their emissions and also meteorological and geophysical data (Fig 3.6).

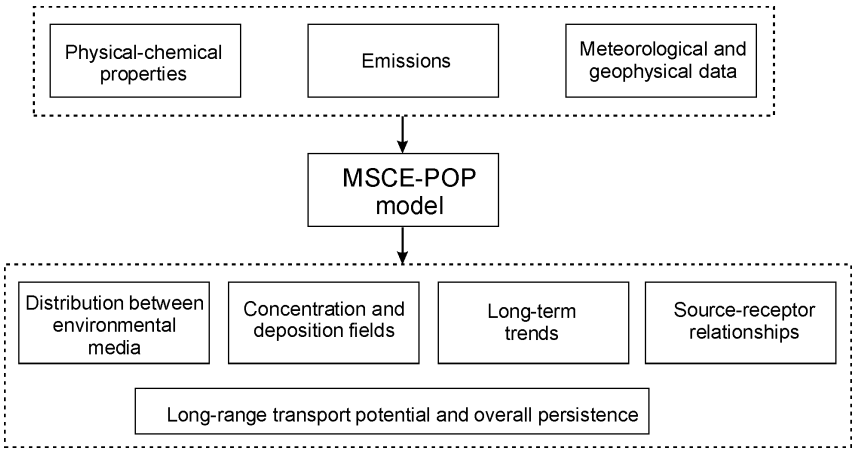

Figure 3.6. *Input and output data of the MSCE-POP multicompartment model*

Output model information includes:

- fields of deposition and concentration in environmental media and long-term trends of contamination in them;
- distribution of a pollutant between environmental media;
- source-receptor relationships;
- long-range transport potential and overall persistence.

The main environmental compartments included in the model are (Fig. 3.7):

- atmosphere;
- soil;
- seawater;
- vegetation;
- sea ice and snow.

It is assumed that POPs are emitted to the atmosphere from which they may be uptaken by the underlying surface (soil, seawater, sea ice/snow, vegetation) or leave the calculation domain as a result of transport. The following processes affecting the long-range transport of POP are included in the model:

The atmosphere:

- transport with advection and diffusion;
- partitioning of a pollutant between the gaseous and particulate phase;
- wet and dry deposition of the particulate and gaseous phase to the underlying surface;
- degradation.

Vegetation:

- gaseous exchange with the atmosphere;
- defoliation.

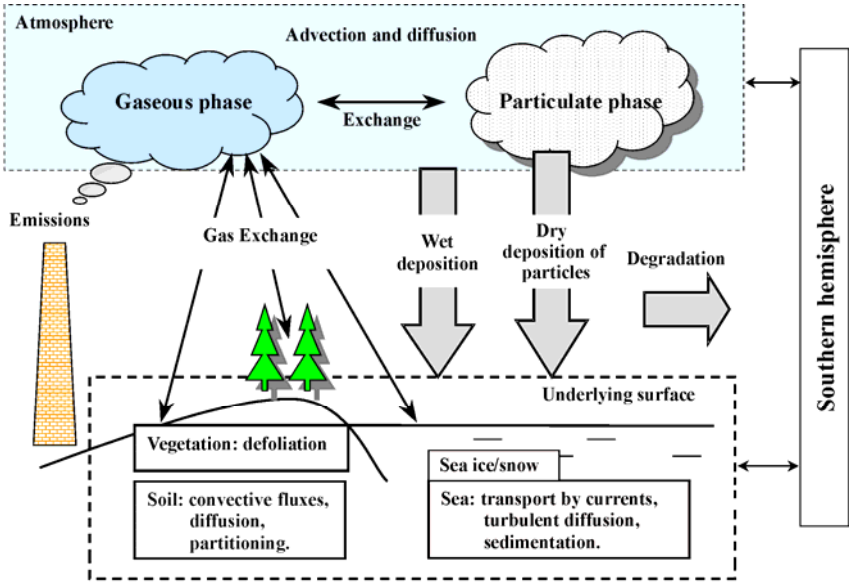

Figure 3.7. *The scheme of processes included into the MSCE-POP hemispheric model*

Soil:

- gaseous exchange with the atmosphere;
- partitioning between the gaseous, solid and liquid phase;
- vertical transport of a pollutant by convective water fluxes and diffusion;
- degradation.

Seawater:

- gaseous exchange with the atmosphere;
- transport of a pollutant by sea currents and turbulent diffusion;
- redistribution between the dissolved and particulate phase;
- sedimentation;
- degradation.

Sea ice/snow:

- accumulation of POPs in the snow and ice medium,
- gas phase exchange between the snow and the atmosphere,
- fluxes into the seawater as a result of snow and ice melting,
- fluxes from the seawater to the ice cover during ice bottom/lateral accretion,
- horizontal transport with drifting ice,
- degradation in the snow pack and ice.

We believe that these processes, included in the current version of the MSCE-POP hemispheric model, are vital for the description of POP transport in the environment. This statement is substantiated by a review of literature and a model sensitivity study. The latter is exemplified in Annexes D, E.

The following sections present the description of individual modules of the MSCE-POP model.

3.3.2. The atmosphere

This section describes processes included in the atmospheric module of the MSCE-POP hemispheric model. These processes are: partitioning of a pollutant between the gaseous and particulate phase; wet and dry deposition of both phase to the underlying surface; and degradation. Advection and diffusion schemes of the model are the same as in the MSCE-Hg-Hem model, which is described in Section 3.2.

Gas/particle partitioning

Characterization of POP partitioning between the gas and particulate phase of a pollutant is performed using subcooled liquid vapour pressure p_{OL} (Pa). According to the Junge-Pankow model [*Junge*, 1977; *Pankow*, 1987] the POP fraction φ adsorbed on atmospheric aerosol particles equals to:

$$\varphi = \frac{c \cdot \theta}{p_{OL} + c \cdot \theta}, \tag{3.31}$$

where c is the constant dependant on the thermodynamic parameters of the adsorption process and on the properties of aerosol particle surface. It is assumed c = 0.17 Pa·m [*Junge*, 1977] for background aerosol;

θ is the specific surface of aerosol particles, m^2/m^3 (θ = $1.5 \cdot 10^{-4}$ m^2/m^3 for background aerosol [*Whitby, 1978*]); to assess the influence of this assumption rough experimental calculations are made (see Annex F).

Parameter p_{OL} is pollutant-dependent and depends greatly on temperature. This dependence essentially affects the long-range transport of a pollutant and is included in the model in the form:

$$p_{OL} = p_{OL}^0 \exp\left[-a_P\left(\frac{1}{T} - \frac{1}{T_0}\right)\right], \tag{3.32}$$

where T is the ambient temperature, K;

T_0 is the reference temperature, K;

p_{OL}^0 is the value of p_{OL} at the reference temperature T_0;

a_P is the coefficient of the vapour pressure temperature dependence, K.

Dry deposition of the particulate phase

Dry deposition flux of the particulate phase F_{dry}^P ($ng/m^2/s$) is a product of dry deposition velocity V_d (m/s) and particle air concentration C_P (ng/m^3) taken at an air reference level coinciding with the middle of the lowest atmospheric layer:

$$F_{dry}^P = V_d C_P, \tag{3.33}$$

where the dry deposition velocity from the reference level z_a is calculated according to the resistance analogy using the equation:

$$V_d = \left(r_a + 1/V_d^{surf} \right)^{-1}. \quad (3.34)$$

Here r_a is the aerodynamic resistance for turbulent transport of a pollutant from z_a to z_b, s/m;

z_b is the height of the surface layer, m;

V_d^{surf} is the surface dry deposition velocity from the surface layer height z_b, which is estimated by special models for different landcover.

Aerodynamic resistance r_a is calculated using the following equation [*Tsyro and Erdman,* 2000]:

$$r_a = \frac{0.74}{\kappa u_*} \left[\ln\left(\frac{z_a}{z_b} \right) - \psi_h\left(\frac{z_a}{L} \right) + \psi_h\left(\frac{z_b}{L} \right) \right], \quad (3.35)$$

where $\kappa = 0.4$ is the van Karman constant;

u_* is the friction velocity, m/s;

ψ_h is the similarity function for heat.

The values of deposition velocity to the underlying surface V_d^{surf} are calculated for sea, soil and forest separately.

<u>*Sea*</u>. Velocity of dry deposition over sea (V_d^{sea}, z_b = 10 m), cm/s is calculated by the equation:

$$V_d^{sea} = A_{sea} u_*^2 + B_{sea}, \quad (3.36)$$

where u_* is the friction velocity, m/s;

A_{sea} and B_{sea} are the constants dependant on the effective diameter of particle-carriers of a considered pollutant.

(regression equation obtained by *M.Pekar* [1996] from [*Lindfors et al.*, 1991] data).

<u>*Soil.*</u> Velocity of dry deposition over soil (V_d^{soil}, z_b = 1 m), cm/s is given as follows:

$$V_d^{soil} = \left(A_{soil} u_*^2 + B_{soil} \right) z_0^{C_{soil}}, \quad (3.37)$$

where as above u_* is the friction velocity;

z_0 is the surface roughness, mm

A_{soil}, B_{soil}, C_{soil} are the constants dependant on effective diameters of particle-carriers of considered POP;

(regression equation obtained by *M.Pekar* [1996] from [*Sehmel*, 1980] data).

<u>*Forest*</u>. Velocity of dry deposition to a forest (V_d^{forest}, z_b = 20 m), (adapted by *L.Erdman* [*Tsyro and Erdman*, 2000] from [*Ruijgrok et al.*, 1997]), m/s:

$$V_d^{forest} = E \frac{u_*^2}{u_h}, \quad (3.38)$$

where u_h is the wind speed at forest height $h = z_b$;

$$E = \alpha\, u_*^{\beta} \left(1 + \gamma \exp\left(\left(RH - 80 \right) / 20 \right) \right) \quad (3.39)$$

is the total collection efficiency for particles within the forest canopy and α, β and γ are the experimental coefficients, depending on effective diameters of particles-carriers.

In the current model version it is assumed that the relative humidity of air is 80% of the average. Wind speed at forest height u_h (m/s) is calculated using the following equation:

$$u_h = \frac{u_*}{\kappa}\left[\ln\left(\frac{z_b - d_0}{z_0}\right) - \psi_m\left(\frac{z_b - d_0}{L}\right) + \psi_m\left(\frac{z_0}{L}\right)\right], \quad (3.40)$$

where κ = 0.4 is the van Karman constant;
d_0 = 15 m is zero-plane displacement;
z_0 = 2 m is the roughness length;
L is the Monin-Obukhov parameter;
ψ_m is the universal correction function for the atmospheric stability for momentum.

Two types of forest are distinguished in the model: deciduous forest and coniferous forest. It is assumed that dry deposition velocities to forest are calculated by Eq. (3.38) for deciduous forests during the vegetative period (only from May to September). For the remaining time, dry deposition velocities for areas covered by deciduous forests are calculated as for soil Eq. (3.37). For areas covered by coniferous forests dry deposition velocities are calculated by Eq. (3.38) throughout the year.

The amount of pollutant deposited to forest is distributed between soil and leaves/needles in accordance with the distribution coefficient K_{vs}, which is pollutant-dependent.

The coefficients A_{sea}, B_{sea}, A_{soil}, B_{soil}, C_{soil}, α, β and γ, as well as the distribution coefficient K_{vs} between soil and leaves/needles for forests, are a part of model parameterization for a particular chemical.

Wet deposition

Wet depositions of the gaseous and particulate phase are distinguished in the model. For the description of gaseous phase scavenging with precipitation, the instantaneous equilibrium between the gaseous phase in the air and the dissolved phase in precipitation is assumed:

$$C_w^d = W_g\, C_a^g\,, \quad (3.41)$$

where C_w^d is the dissolved phase concentration in precipitation water, ng/m^3;
C_a^g is the gaseous phase concentration in air, ng/m^3;
$W_g = 1/K_H$ is the dimensionless washout ratio for the gaseous phase;
K'_H is the dimensionless Henry's law constant.

The latter is temperature-dependent and is given by the equation:

$$K'_H = \frac{H_0}{RT}\exp\left[-a_H\left(\frac{1}{T} - \frac{1}{T_0}\right)\right], \quad (3.42)$$

where T is the ambient air temperature, K;
T_0 is the reference temperature;
R is the universal gas constant, J/(mol·K),
a_H is the coefficient of Henry's law constant temperature dependence, K;
H_0 is the value of Henry's law constant at reference temperature, Pa·m^3/mol.

For the description of particle bound phase scavenging with precipitation, the washout ratio determined experimentally is used:

$$C_w^s = W_p C_a^p, \tag{3.43}$$

where C_a^p is the particle bound phase concentration in the air surface layer, ng/m^3;
C_w^s is the suspended phase concentration in precipitation water, ng/m^3;
W_p is the dimensionless washout ratio for the particulate phase.

Since the meteorological data used in the model provide information for precipitation intensity in all vertical layers, wet deposition is calculated in each layer both for the gaseous and particulate phase of the pollutant.

The constants H_0, a_H, and W_g are parameters unique to each POP.

Degradation

The degradation process in the atmosphere is described by the reaction of a pollutant with OH radicals:

$$\frac{dC}{dt} = -k_{air} \cdot C \cdot [\mathrm{OH}], \tag{3.44}$$

where C is the pollutant concentration in air (gaseous phase), ng/m^3;
[OH] is the concentration of OH radical, molecules/cm^3;
k_{air} is the degradation rate constant for air, cm^3/s/molecules,

whose temperature dependence is provided by the equation:

$$k_{air} = A \cdot \exp(-E_a / RT), \tag{3.45}$$

where A is the exponential multiplier;
E_a is the activation energy;
R is the universal gas constant;
T is the ambient temperature.

Parameters A and E_a depend on pollutant properties.

This equation is applied for the gaseous phase of a pollutant. Currently the process of degradation of a pollutant associated with particles is not included in the model due to lack of information on this topic. It should be mentioned that degradation under Arctic conditions (low temperatures, short daylight) is insignificant in comparison with that in the middle latitudes.

OH radical concentrations in the atmosphere vary substantially depending on many factors (latitude, cloudiness, day time, season, some atmospheric properties, etc.). At present, in the model as a first approximation, OH radical concentrations have no diurnal variations and depend only on the season. According to [*Yu Lu and Khall*, 1991] the following values were accepted:

Winter [OH] = $9 \cdot 10^4$, fall, spring [OH] = $8 \cdot 10^5$, summer [OH] = $2 \cdot 10^6$.

To assess the influence of this assumption rough experimental calculations are made (see Annex F). Temporal and spatial variations of this parameter will be taken into account in the model in the near future.

Gaseous exchange with underlying surface

Gaseous exchange between the atmosphere and underlying surface is based on the resistance analogy. Gaseous exchange takes place with soil, vegetation, seawater and sea ice (snow). Its description is given in corresponding sections devoted to the mentioned media (types of underlying surface).

3.3.3. Soil

The soil module is based on the model developed by of *C.M.J. Jacobs and W.A.J. van Pul* [1996].

In the model, soil is separated into five horizontal layers of different thicknesses. The thicknesses of the layers are chosen individually for each pollutant considered, namely, for PCBs these are Δz_i = 0.01, 0.05, 0.2, 0.8 and 3 cm from above, and for γ-HCH – Δz_i = 0.5, 0.5, 1, 2 and 11 cm [*Shatalov et al*., 2001]. In the current version of the model the following processes are included: partitioning of the pollutant between various phases in soil; vertical diffusion and advection with water flux; gaseous exchange with the atmosphere; and the degradation of the pollutant.

Partitioning in soil

The total volume concentration in soil C is expressed via the mass concentration C^s of a pollutant sorbed by the soil matter, the volume concentration C^d of a pollutant dissolved in the soil water, and the gas-phase volume concentration C^g of a pollutant in the soil air, ng/m^3:

$$C = \rho_s C^s + \theta C^d + aC^g \tag{3.46}$$

where ρ_s = 1350 is the bulk soil density, kg/m^3;
θ = 0.3 is the volumetric water content in soil;
a = 0.2 is the volumetric air content in soil.

The concentration in each phase may be represented by C using the soil partitioning coefficients R_s, R_d and R_g :

$$C = R_s C^s = R_d C^d + R_g C^g, \tag{3.47}$$

where $R_d = \rho_s K_d + \theta + a K_H$; $R_s = R_d / K_d$; $R_g = R_d / K'_H$;
$K_d = f_{OC} K_{OC}$ is the slope of the adsorption isotherm;
f_{OC} is the fraction of organic carbon in soil;
K_{OC} is the organic carbon distribution coefficient;
K'_H is the dimensionless Henry's law constant (see above).

Vertical transport

The migration of a pollutant over the vertical profile in soil is assumed to be due to diffusion and transport with the convective water flux J_w (equal to mean annual precipitation intensity h_p, m/c). The corresponding equation is:

$$\frac{\partial C}{\partial t} + \frac{J_w}{R_d}\frac{\partial C}{\partial z} = D_E \frac{\partial^2 C}{\partial z^2}, \tag{3.48}$$

where D_E is the effective gas-liquid diffusion coefficient, m^2/s.

The coefficient D_E is determined by:

$$D_E = \frac{\xi_g D_g}{R_g} + \frac{\xi_l D_l}{R_d}, \tag{3.49}$$

where D_g, D_l are the molecular diffusion coefficients for gas and liquid;

$\xi_g = a^{10/3}/\phi^2$, $\xi_l = \theta^{10/3}/\phi^2$ are gas and liquid tortuosity factors;

ϕ is the porosity of soil (assumed ϕ = 0.5).

Gaseous exchange with the atmosphere

Gaseous exchange between soil and the atmosphere is parameterized using the resistance analogy.

The gaseous flux of POP from the atmosphere into the soil is driven by the difference between atmospheric gas concentration C_a^g at the air reference level z_a (equal to half the height of the lower atmospheric layer) and the soil gas-phase concentration C_s^g at the soil reference level at depth z_s=Δz_1/2 (Δz_1 – is the upper soil layer thickness). In the course of pollutant transport from the air reference level to the soil reference level it overcomes three resistances (see Fig. 3.8).

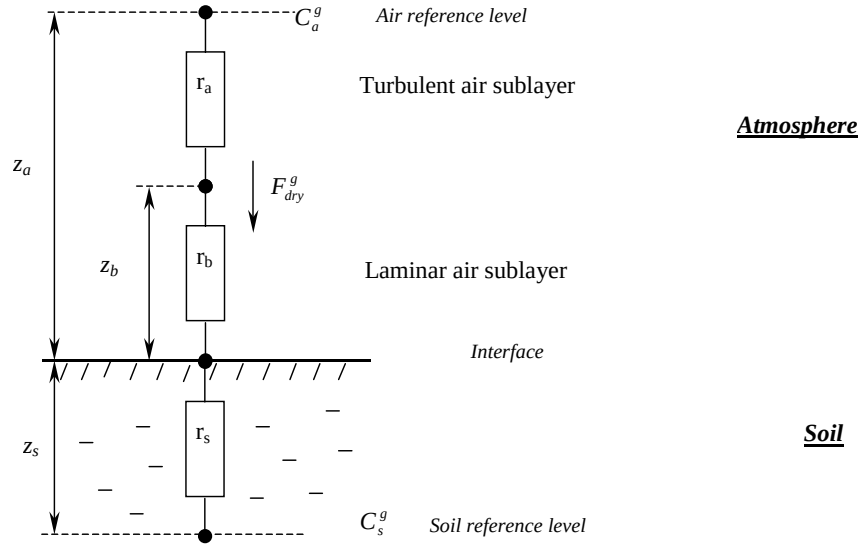

Figure 3.8. *Resistance scheme used for the description of gaseous exchange between atmosphere and the soil*

- Turbulent air sublayer resistance r_a, s/m that is, the resistance to transport through the turbulent air sublayer (from z_a to z_b. The latter is laminar sublayer height);
- Laminar surface air sublayer resistance r_b, s/m that is, the resistance to transport through the laminar surface air sublayer (z_b) to the interface;

- Surface soil resistance r_s, s/m that is, the resistance to transport from the surface soil interface to the soil reference level (z_s).

Hence, the formula for atmosphere/soil flux is:

$$F_{dry}^{g} = \frac{C_a^g - C_s^g}{r_a + r_b + r_s}, \tag{3.50}$$

where r_a is given by formula (3.35), and:

$$C_s^g = \frac{C(z_1)}{R_g} \frac{2D_E / \Delta z_1}{\left(2D_E / \Delta z_1 + J_w / R_d\right)}, \tag{3.51}$$

$$r_s = \frac{1}{R_g\left(2D_E / \Delta z_1 + J_w / R_d\right)}, \tag{3.52}$$

$$r_b = \frac{2}{\kappa u_*}\left(\frac{Sc}{\Pr}\right)^{2/3}, \tag{3.53}$$

where $Pr = 0.71$ is the Prandtl number;
$Sc = n/D_a$ is the Schmidt number;
$n = 1.5 \cdot 10^{-5}$ is the kinematic viscosity of air, m^2/s;
D_a is the molecular diffusion coefficient of a pollutant in air, m^2/s;
D_E is the effective molecular gas-liquid diffusion coefficient, m^2/s;
J_w is the convective water flux equal to mean annual precipitation intensity, m/c;
R_d, R_g are the soil partitioning coefficients, dimensionless;
u_* is the friction velocity, m/s.

Degradation

The degradation process in soil is described as a first-order process by the equation:

$$\frac{dC}{dt} = -k_{soil} C, \tag{3.54}$$

where C is the pollutant concentration in soil, ng/m^3;
k_{soil} is the degradation rate constant for soil, s^{-1}.

The degradation rate constant k_{soil} is a part of model parameterization for a given pollutant. It is assumed, as a first approximation, that doubling of the degradation rate constant occurs with each 10K temperature increase. This temperature dependence was adapted from [*Lammel et al.*, 2001].

3.3.4. Vegetation

Three types of vegetation are distinguished in the model: coniferous forest, deciduous forest, and grass. Coefficients governing exchange processes between the atmosphere and vegetation are determined separately for each of the above vegetation types. Furthermore, we consider forest litter as an intermediate medium between vegetation and soil. In essence this medium can be viewed as an upper soil layer. The description of these media is placed in this section.

Gaseous exchange with the atmosphere

The equation describing atmosphere/vegetation exchange has the following form:

$$\frac{dC_V}{dt} = \frac{1}{R_{tot}}(C_a^g - C_V / K_{Va}), \tag{3.55}$$

where C_a^g is the air concentration of a pollutant;

C_V is the concentration in vegetation of a given type;

K_{va} is the bioconcentration factor *(BCF)*;

R_{tot} is the total resistance to the gaseous exchange given by the formula:

$$R_{tot} = R_a + a_V / k, \tag{3.56}$$

where R_a is the aerodynamic resistance of the turbulent atmospheric layer (see formula 3.27 above);

k is the mass transfer coefficient, m/s;

a_V is the specific surface area of vegetation, m^2/m^3 (assumed value is 8000, see [*Duyzer and van Oss*, 1997]).

The total amount of pollutant in vegetation of a given type in a certain grid cell is then expressed by the equation:

$$Q = C_V \frac{S \cdot \mathrm{LAI}}{a_V}, \tag{3.57}$$

where S is the area covered by vegetation of a given type within a grid cell;

LAI is the particular leaf area index for the considered type of vegetation.

Parameterization of BCF. The bioconcentration factor is determined by the following equation [*McLachlan and Horstmann*, 1998]:

$$K_{Va} = mK_{OA}^n, \tag{3.58}$$

where K_{OA} is the partitioning coefficient between octanol and air;

m, n are the regression coefficients presented in Table 3.1.

Table 3.1. *Regression parameters for Equation (3.58)*

	Grass [*Thomas et al.*, 1998]	Forest, [*McLachlan and Horstmann*, 1998],	
		Coniferous	Deciduous
m	22.91	38	14
n	0.445	0.69	0.76

While calculating BCF using Eq. (3.58) the temperature dependence of K_{OA} should be taken into account. In the model it is assumed that:

$$K_{OA} = K_{OA}^0 \exp\left[a_K\left(\frac{1}{T} - \frac{1}{T_0}\right)\right], \tag{3.59}$$

where as earlier T_0 = 283.15 K is the reference temperature;

K_{OA}^0 is the K_{OA} value at the reference temperature;

a_K is the coefficient of K_{OA} temperature dependence, K.

Parameterization of the mass transfer coefficient k. According to [*Pekar et al.,* 1999], the mass transfer coefficient is directly proportional to the value of K_{OA}. Hence, for the evaluation of the temperature dependence of *k* the following formula can be used:

$$k = k_0 \exp\left[a_K \left(\frac{1}{T} - \frac{1}{T_0} \right) \right], \tag{3.60}$$

where k_0 is the *k* value at the reference temperature, based on the data given in [*McLachlan and Horstmann,* 1998] for forests and in [*Pekar et al.,* 1999] for grass.

The values of K_{OA}^0 and a_K are pollutant-dependent and their values are given in Chapter 2.

Defoliation and transport to soil from forest litter

A description of the defoliation process is also included in the model. It is assumed that part of the pollutant transported from vegetation to the forest litter is proportional to the decrease of leaf area index. For coniferous trees defoliation was described as a first-order process with a life-time $T_{1/2}$ = 2 years. In view of the permanent character of seasonal LAI variation in the tropical zone, for all types of vegetation in that zone defoliation was described as a first-order process with a life-time $T_{1/2}$ = 0.5 years. Mentioned life-times are preliminary and may be refined in the future.

The transmission of a pollutant from fallen leaves to the underlying soil was described as a first order process with the life-time depending on the latitude. On the base of the Technical Note 1/2002 [*Vassilyeva and Shatalov*, 2002], the life-time for the polar calculation cells was selected as $T_{1/2}$ = 20 years, for the equatorial the life-time was assumed as $T_{1/2}$ = 0.1 year. Between polar and equatorial zones, life-time is calculated using linear dependence in logarithmic scale. We admit that this is rather crude spatial parameterization, which may be improved in the future.

Degradation

There is very little data on degradation rates of considered chemicals in vegetation. For this reason, the degradation process in vegetation is not considered at present. A more detailed discussion of this question with rough estimation of degradation rates in vegetation for some POPs can be found in [*Pekar et al.*, 1999]. On the basis of preliminary investigations, the degradation process in forest litter was introduced to the model as a first-order process with a degradation constant rate two times higher than of that in soil.

3.3.5. Seawater

This section contains a general description of the processes included in the seawater module of the current version of the hemispheric MSCE-POP model.

The calculation domain is divided into 15 vertical layers with depths of 12.5, 37.5, 65, 105, 165, 250, 375, 550, 775, 1050, 1400, 1900, 2600, 3500, 4600 metres. Horizontal resolution is 1.25°x1.25°, that is, two times less than the atmospheric one. More detailed spatial resolution for the ocean module allows for consideration of dynamical processes in the ocean on appreciably smaller scales than in the atmosphere. For example, this spatial resolution produces a reasonable description of sea currents nearby the coastal line.

Basic equation

The equation for the dynamics of total concentration, including a description of advection, turbulent diffusion, degradation and sedimentation can be written as follows:

$$\frac{Dc}{Dt} = K_H \Delta_H c + \frac{\partial}{\partial z}(K_V \frac{\partial c}{\partial z}) - v_{sed} \frac{\partial c_p}{\partial z} - k_d c \,, \tag{3.61}$$

where c, c_p are POP total and particulate phase concentrations;

$\frac{D}{Dt}$ is the total derivative in time;

Δ_H is the Laplace operator in horizontal variables;

$K_V(z)$ and K_H are the coefficients of vertical and horizontal diffusion;

v_{sed} is the sedimentation rate constant, which is estimated by the Stokes formula:

$$v_{sed} = \frac{g(\rho_p - \rho_w){d_p}^2}{12\mu} \tag{3.62}$$

where g is gravitational acceleration, m/s^2;

ρ_p is mean density of particles, kg/m^3;

ρ_w is water density, kg/m^3;

d_p is the diameter of seawater particles, m;

μ is dynamic viscosity of seawater, kg/m/s.

Fields of sea current velocities, and the depth of the upper mixed layer, used to calculate vertical turbulent diffusion, are taken from the ocean dynamic model.

POP partitioning between different phases

POP redistribution between the dissolved phase, and the phase associated with particles, essentially affects the dynamics of POP concentration fields in the marine environment. Under the condition of instantaneous phase equilibrium establishment it is possible to consider that the relationship is always fulfilled:

$$c^p = k^p c^d \tag{3.63}$$

where c^p is the concentration of POP sorbed on particles;

c^d is the concentration of POP dissolved in water;

k^p is the partition coefficient between the particle and dissolved phase.

In its turn k^p may be estimated by the expression:

$$k^p = k_p^o K_p c_{prt} \tag{3.64}$$

where k_p^o is the fraction of organic matter in a particle;

K_p is the equilibrium constant for sorption/desorption processes (proportional to the octanol-water coefficient K_{OW});

C_{prt} is particle concentration.

Air/seawater mass exchange

For POP flux through the sea surface the following expression is used

$$F_z\big|_{z=0} = \alpha_1(c_a^g / K'_H(T) - c^d)((1-\alpha_2)D_w / \delta + \alpha_2 K_{HR}\dot{h}_f) + F_{gw} + F_{pd} + F_{pw}, \quad (3.65)$$

where:

$$\delta = \delta_0 \exp(-0.15 \cdot U_a),$$
$$\alpha_1 = 1.75 - 0.75\exp(-0.18 \cdot U_a),$$
$$\alpha_2 = 1 - \exp(-0.01 \cdot U_a).$$

c_a^g is the POP gas-phase concentration in the lower layer of the atmosphere;
c^d is the dissolved POP concentration in upper layer of the sea;
$K'_H(T)$ is the dimensionless Henry's law constant depending on temperature;
D_w is the molecular diffusion coefficient in water;
δ_0 is the surface molecular layer depth at zero wind speed;
U_a is the wind speed absolute value near the surface;
$\dot{h}_f$ is the foam settling rate at the sea surface;
F_{gw} is the POP gas-phase flux with precipitation;
F_{pd} is the flux of POP associated with particles in the atmosphere as a result of particle dry deposition;
F_{pw} is the flux of POP associated with particles in the atmosphere as a result of particle washout with precipitation;
α_1 is the coefficient introduced for the description of surface sea area increase due to wave disturbance;
α_2 describes the relative sea surface area covered with foam at strong wind.

A more detailed description of these processes is given in [*Strukov et al.*, 2000].

Further development of the hemispheric model is associated with the refinement of the partitioning of a pollutant between the dissolved and particle phase, as well as sedimentation process. These processes strongly influence the fate of pollutants in the marine environment, and affect air concentrations over sea through gaseous exchange fluxes.

POP transport with ice cover

While POP transport modeling takes place within the scale of the globe it is necessary to consider the effect of ice coverage over the vast areas of the polar region. Sea ice plays the role of a screen between the seawater and the atmosphere. At the same time POP may be accumulated in ice itself and in the snow on it. The process of POP exchange with the atmosphere takes place on the upper snow-ice surface. When snow and ice are melting on the upper surface, or ice is melting on the lower or lateral surfaces, POP passes to the water environment. In the case of ice accretion on the lower or lateral ice surfaces, POP can penetrate into the ice medium. Furthermore, POP trapped by the sea ice and snow may be transported with ice drift. The scheme of basic processes in the atmosphere/snow/ice/seawater system is presented in Figure 3.9.

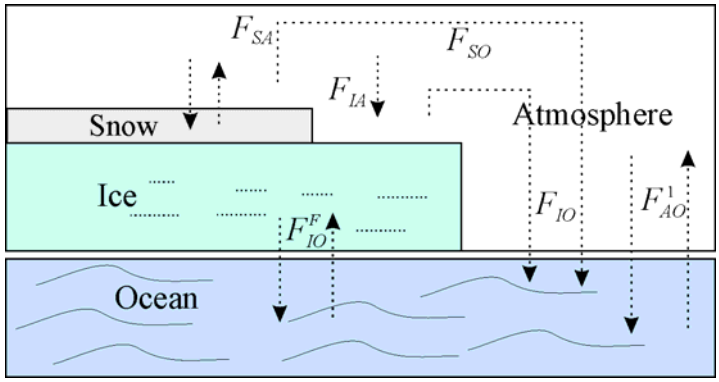

Figure 3.9 *The scheme of POP fluxes in the system atmosphere-snow/ice-seawater*

F_{SA} – flux between the atmosphere and the snow pack (snow on the ice surface), F_{SO} - flux from the upper surface of the snow pack into seawater (snow on the ice surface), F_{IA} – flux from the atmosphere onto the upper ice surface (no snow), F_{IO} – flux into the seawater from the upper ice surface (no snow), F_{IO}^{p} – flux between the seawater and the ice medium (particle phase only). Fluxes downward are considered to be positive.

POP flux between the atmosphere and seawater without sea ice may be represented as:

$$F_{AO}^{0} = F_z\big|_{z=0} = F_d^g + F_w^g + F_d^p + F_w^p \,, \tag{3.66}$$

where F_d^g is POP gas phase flux between the seawater and the atmosphere;

F_w^g is the gas phase flux from the atmosphere to the seawater with precipitation;

F_d^p is the atmospheric dry deposition flux of POP with particles to the seawater;

F_w^p is the flux of POP with particles depositing with precipitation.

To take into account the screening effect of sea ice, F_{AO}^{0} should be substituted for the expression:

$$F_{AO}^{1} = F_{AO}^{0}(1-A)\,, \tag{3.67}$$

where A is ice compactness in dimensionless units ($A = S_i / S$, S_i – ice square on sea square S).

POP molecules in the snow-ice environment may be found in different physical states: in the gaseous phase, in snow-ice pores, sorbed on surface ice crystals (the surface phase), incorporated into organic particles contained in the snow-ice medium (the particle phase), dissolved in water, if any, in the snow or ice medium. As a first approximation the following simplifications are made:

- equilibrium between POP different phases is instantly established;
- snow and ice are not saturated by water, i.e. the POP aqueous phase is absent in the ice coverage;
- POP entering the ice surfaces with the help of active vertical mixing mechanisms (hummocking and others) are distributed in the ice medium.

In accordance with these assumptions the total concentration of the gaseous and surface phase (kg/m^3) in snow pack is denoted as c_{sn}; the total concentration of the gaseous and surface phase in the ice medium (kg/m^3) – as c_{ic}; concentration of the particle phase in the snow (kg/m^3) – as c_{sc}^{p} ; and the concentration of the particle phase in the ice thickness (kg/m^3) – as c_{ic}^{p}. The thickness of the snow cover on the ice and the ice thickness are denoted by h_{sn} and h_{ic}, respectively. The values of h_{sn}, h_{ic},

may depend on the horizontal co-ordinates λ, φ and time t concentration. Values c_{sn}, c_{in}, c^p_{sn}, c^p_{ic} may also depend on the vertical co-ordinate z. In view of the essentially smaller vertical scale, in comparison with the horizontal, vertically averaged values of concentrations c_{sn}, c_{in}, c^p_{sn}, c^p_{ic} will be considered. The area specific mass of different POP phases for the snow and ice, in accordance with ice compactness, may be represented by the expression:

$$m_{sn} = Ac_{sn}h_{sn}\,,\quad m^p_{sn} = Ac^p_{sn}h_{sn}\,,\quad m^p_{ic} = Ac^p_{ic}h_{ic}\,,\quad m_{is} = Ac_{is}h_{ic} \tag{3.68}$$

The balance equation of the considered POP fluxes for snow and ice medium and for the ice surface may be written as:

- for the sum of gaseous and surface phases of the snow pack:

$$\frac{dm_{sn}}{dt} = (F^{'g}_d + F^g_w + F_{SO})A - F_{Sd}\,, \tag{3.69}$$

where $F^{'g}_d$ is the atmospheric dry deposition flux of gaseous POP between the atmosphere and snow;
F^g_w is the atmospheric wet deposition flux of gaseous POP from the atmosphere (previously defined);
F_{SO} is the flux of the gaseous and surface phases of POP from the upper snow surface into seawater;
F_{Sd} is the degradation rate of gaseous and surface phases in snow.

- for the particle phase in the snow pack:

$$\frac{dm^p_{sn}}{dt} = (F^p_d + F^p_w + F^p_{SO})A - F^p_{Sd}\,, \tag{3.70}$$

where F^p_d, F^p_w are the atmospheric dry and wet deposition fluxes of POP with particles (previously defined);
F^p_{SO} is the flux of the particle phase of POP from the upper snow surface into seawater;
F^p_{Sd} is the degradation rate of the particle phase in snow.

- for the sum of the gaseous and surface phase in the ice:

$$\frac{dm_{is}}{dt} = (F^g_w + F_{IO})A - F_{Id}\,, \tag{3.71}$$

where F_{IO} is the flux of the surface phase of POP from the upper ice surface into seawater;
F_{Id} is the degradation rate of the surface phase in ice.

The gaseous phase in the ice medium is neglected due to the small volume of the pores in the ice.

- for the particle phase in the ice medium:

$$\frac{dm^p_{ic}}{dt} = (F^p_d + F^p_w + F^p_{IO})A - F^p_{Id}\,. \tag{3.72}$$

where F^p_{IO} is the flux of the particle phase of POP between bottom and lateral ice surfaces and seawater;
F^p_{Id} is the degradation rate of the particle phase in ice.

In these balance equations the total derivative for the two-dimensional problem is taken into consideration. Horizontal POP mass transport is realized with the ice drift along velocity fields *(u_{ic}, v_{ic})*, where u_{ic} – meridian, v_{ic} – zonal components of ice velocities.

The undefined mass fluxes in the right sides of Eq. (3.69) – (3.72) are represented by the following relationships.

The flux of the gaseous phase between the atmospheric and snow pack.

$$F_d^{'g} = \frac{(c_a^g - c_{surf})}{r + r_{surf}} . \tag{3.73}$$

Here c_a^g is the gas phase concentration in the atmosphere;

r is resistance to the atmospheric flux;

$r_{surf} = \frac{h_{sn}}{2\phi_{sn}^{4/3} D_g}$; $c_{surf} = c_{gsn} = c_{sn} / R_{sn}^g$;

D_g is the POP molecular diffusion coefficient in gas;

$\phi = \frac{\rho_w - \rho_{sn}}{\rho_w}$ is snow porosity;

ρ_w, ρ_{sn} are water and snow density respectively,

The expression for $F_d^{'g}$ may be derived from the model of POP exchange between soil and the atmosphere [*Pekar et al.,* 1998] under the condition that the water phase is absent. The coefficient R_{sn}^g in the relationship for c_{surf} is expressed through snow porosity, snow density, specific surface area of crystals s_{sn} and the coefficient of equilibrium between the gas and surface phase K_{ia} [*Koziol and Pudykiewicz,* 2001].

$$R_{sn}^g = \phi + \rho_{sn} s_{sn} K_{ia} \tag{3.74}$$

The values K_{ia} are connected with the POP solubility C_W and Henry's law constant:

$$\log(K_{ia}) = 0.769 \cdot \log(C_W) - 5.966 - \log(K'_H(T_{sn})) , \tag{3.75}$$

where T_{sn} is snow temperature.

- For the sum of gaseous and surface phase fluxes from snow surface into the seawater (snow on the ice surface), presuming that in the majority of cases melting water leaks into the seawater through cracks and ice-holes on the ice cover (because of ice compactness A almost everywhere is less than 1):

$$F_{SO} = -dh_{sn} c_{sn} \quad \text{at} \quad h_{sn} > 0 , \tag{3.76}$$

where dh_{sn} is snow cover melting rate.

- For the particle phase flux between the seawater and snow with the same assumptions

$$F_{SO}^p = -dh_{sn} c_{sn}^p \quad \text{at} \quad h_{sn} > 0 \tag{3.77}$$

- For the surface phase flux into seawater from the upper ice surface.

$$F_{IO} = -dh_{is} c_{ic} \quad \text{at} \quad h_{is} > 0, \tag{3.78}$$

where dh_{is} is the ice melting rate on the upper ice surface.

- For the particle flux into seawater from the upper ice surface.

$$F^p_{IO} = -dh_{is} c^p_{ic} \quad \text{at} \quad h_{is} > 0, \tag{3.79}$$

For the particle phase between the ice medium and seawater on the bottom / lateral surfaces of ice:

$$F^p_{IO} = -dh_{ib} c^p_{ic} \qquad \text{at} \qquad dh_{ib} > 0 \quad \text{(melting)} \tag{3.80}$$

$$F^p_{IO} = -dh_{ib} c^p_{w} \qquad \text{at} \qquad dh_{ib} \le 0\ , \quad \text{(accretion)}$$

where dh_{ib} is the ice melting rate on the lower ice surface;

c^p_w is concentration of the particle phase in the water surface layer.

It is considered that at ice bottom/lateral surfaces accretion POP gas and surface phase do not enter the new ice ("freezing" effect). POPs on particles in water enter the forming ice with the particles. The availability of organic particles trapped by sea ice with POP adsorbed molecules is confirmed by numerous observations [*Pfirman et al.,* 1995].

POP degradation rates are represented by appropriate linear dependence on POP concentration:

$$F_{Sd} = k_{snd} m_{sn}, \quad F^p_{Sd} = k^p_{snd} m^p_{sn}\ , \quad F_{id} = k_{icd} m_{ic}, \quad F^p_{Id} = k^p_{icd} m^p_{ic}\ , \tag{3.81}$$

where k_{snd}, k^p_{snd}, k_{icd}, k^p_{icd} are the degradation rate constants of a substance.

Initial data for modeling, namely, fields of ice compactness, the snow cover and ice thicknesses, their melting rates, and surface temperatures are described in Section 3.9. They are calculated on the basis of the ice dynamic model, which is described in Annex E.

3.4. Meteorological data

The System of Diagnosis of the Lower Atmosphere (SDA) developed by Hydrometeorological Centre of Russia [*Frolov et al.*, 1994; *Rubinstein et al*., 1997,1998; *Frolov et al.*, 1997 a,b,c] provides a set of meteorological data for the hemispheric multi-compartment models. The list of these parameters is presented in Table 3.2. The horizontal resolution of information produced by SDA system is 2.5ºx2.5º. Along the vertical σ-coordinates are used with 9 layers up to the level of 0.26 hPa.

The SDA system consists of the following main units:

- unit of initial data including the control and correction of errors,
- unit of boundary conditions,
- hydrodynamic prognostic model,
- post-processing unit.

Table 3.2. *Meteorological parameters supplied by the SDA system for the Northern Hemisphere with resolution of 2.5ºx2.5º*

Parameter	Notation	Type
Wind velocity	V_Λ, V_Φ	bulk
Air temperature	T_a	bulk
Surface pressure	p_s	surface
Precipitation rate	I_p	bulk
Water vapour mixing ratio	q_w	bulk
Large-scale cloudiness	C_L	bulk
Convective cloudiness	C_C	bulk
Surface temperature	T_s	surface
Vertical eddy diffusion coefficient	K_z	bulk
Roughness of the underlying surface	z_0	surface
Friction velocity	u_*	surface
Monin-Obukhov length	L_{MO}	surface
Soil humidity	M_s	surface
Snow cover height	h_s	surface

3.5. Land cover data

Land cover information is used for correct description of deposition and exchange processes between atmosphere and different types of underlying surface. For this purpose we use 24-category USGS Land Use/Land Cover dataset obtained from NCAR Mesoscale Modeling System (MM5) [*Guo and Chen*, 1994]. This selection is conditioned by the availability of more detailed information on underlying surface types with high spatial resolution (10'x10'). Each grid cell is characterized by several types of surface proportional their area. Table 3.3 contains the description of USGS Land Use/Land Cover System Legend.

Since the formulation of the models described in this report does not require detailed specification of data on the underlying surface, the original 24-categories of land cover were reduced to six general categories (deciduous forests, coniferous forests, grassland, urban and built-up land, bare land and glaciers, water bodies) and redistributed over the model grid.

As an example we present here the spatial distribution of two land cover categories from reduced set: deciduous forests and grassland within the Northern Hemisphere (Fig. 3.10).

Table 3.3. *USGS Land Use/Land Cover System Legend*

No	Description
1	*Urban and Built-Up Land*
2	*Dryland Cropland and Pasture*
3	*Irrigated Cropland and Pasture*
4	*Mixed Dryland/Irrigated Cropland and Pasture*
5	*Cropland/Grassland Mosaic*
6	*Cropland/Woodland Mosaic*
7	*Grassland*
8	*Shrubland*
9	*Mixed Shrubland/Grassland*
10	*Savanna*
11	*Deciduous Broadleaf Forest*
12	*Deciduous Needleleaf Forest*
13	*Evergreen Broadleaf Forest*
14	*Evergreen Needleleaf Forest*
15	*Mixed Forest*
16	*Water Bodies*
17	*Herbaceous Wetland*
18	*Wooded Wetland*
19	*Barren or Sparsely Vegetated*
20	*Herbaceous Tundra*
21	*Wooded Tundra*
22	*Mixed Tundra*
23	*Bare Ground Tundra*
24	*Snow or Ice*

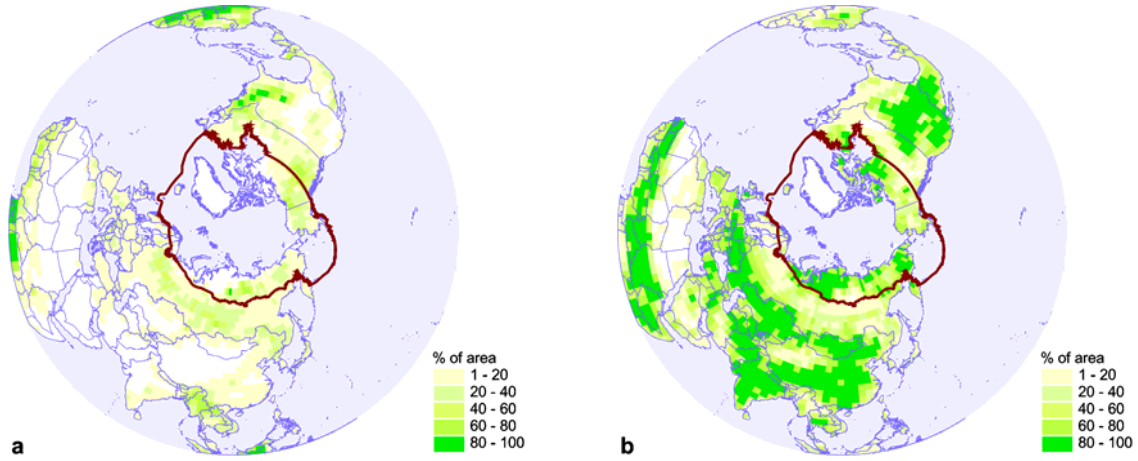

Figure 3.10. *Fraction of the area covered by deciduous forests (a) and grassland (b) in the Northern Hemisphere*

3.6. Leaf Area Index (LAI)

Leaf Area Index (LAI) data set is used for the description of POP gaseous exchange between the atmosphere and vegetation. The Leaf Area Index for a given grid cell implies the ratio between the area of leaves in this cell to its total area (m^2/m^2). The geographically resolved leaf area index data with monthly resolution was adopted from CD-ROM of NASA Goddard Space Flight Center [*Sellers et al*., 1994, 1995] and translated from 1°×1° to 2.5°×2.5° model grid. Consistency of these data in relation to the land cover information was investigated by correlation analysis.

3.7. Chemical reactants data

As it was mentioned in Section 3.2 mercury species take part in chemical reactions of oxidation and reduction both in the gaseous and aqueous phase. To describe chemical transformations one should know spatial and temporal distribution of the reactant concentrations (such as ozone, sulfur dioxide and hydroperoxy radical) in the atmosphere.

Global monthly mean data on ozone, SO_2 concentration in the atmosphere were kindly provided by Dr. Malcolm Ko [*Wang et al.*, 1998; *Chin M. et al.*, 1996]. For hydroperoxy radical (HO_2) we used monthly mean data from Dr. Clarissa Spivakovsky [*Spivakovsky et al.*, 2000]. The original data were interpolated to the model grid for the Northern Hemisphere. Air concentrations of HO_2 were decreased by a factor of 10 in the cloud environment to account for its reduced photochemical activity and heterogeneous chemistry within clouds [*Seigneur et al*., 2001]. Besides, HO_2 concentrations were assumed to be zero at night. The resulted data are briefly described below.

Spatial distribution of ozone concentration in the lowest model layer is demonstrated in Figure 3.11. As seen from the figure elevated values of ozone concentration occur in the middle latitudes around the Northern Hemisphere. The highest ozone concentrations correspond to elevated regions of the Earth surface (within the model grid resolution): the Himalayas, the Rocky Mountains, and Greenland etc. Figure 3.12 shows vertical profiles of ozone concentration in the atmosphere. Each line of the plot demonstrates mean annual ozone concentration averaged along a latitude as a function of altitude

above the sea level. Blue, green, and red lines correspond to the North Pole, 45 °N, and the Equator respectively. According to the figure, ozone concentration increases with altitude in all cases. Besides, the increment is greater for high latitudes than for low ones. Thus, one can expect more intensive mercury oxidation by ozone at the upper troposphere.

Figure 3.13 shows spatial distribution of sulfur dioxide concentration in the surface air of the Northern Hemisphere. The highest concentrations of SO_2 correspond to the most industrially loaded regions such as Europe, the eastern part of North America, Far East and etc. As it is shown in Figure 3.14 SO_2 concentration decreases with altitude practically at all latitudes (except slight growth at high altitudes over the equator). The elevated value of SO_2 concentration in the ground air of the middle latitudes (green line) reflects location of main sulfur sources.

Spatial distribution of hydroperoxy radical HO_2 in the surface air of the Northern Hemisphere is shown in Figure 3.15. As seen from the figure there is well pronounced gradient of HO_2 concentrations from high latitudes to low ones. Besides, concentrations are more significant over land than over the ocean. Vertical distribution of HO_2 concentration (Fig. 3.16) has maximum at approximately 4-5 km altitude for all latitudes. Since dissolved in cloud water HO_2 takes part in aqueous-phase reactions of mercury reduction, one can expect more intensive reduction processes in low latitudes over land.

The model chemistry considers both gaseous- and aqueous-phase oxidation of elemental mercury by chlorine (Cl_2). Currently, the direct production of Cl_2 is very poorly characterized. As it is mentioned in [*Keen et al*., 1999] sea-salt aerosol is the major source of reactive *Cl* gases (particularly Cl_2) in the global troposphere. Average Cl^- content as sea-salt near the sea surface is estimated to be in the range 50-250 nmol Cl^- m^{-3}. Besides, according to the results of general circulation modeling [*Erickson et al.*, 1999] average annual sea-salt Cl^- concentration varies in the Northern Hemisphere from about 150 nmol Cl^- m^{-3} near the equator up to 500 nmol Cl^- m^{-3} in the Northern Atlantic. Following *C. Seigneur et al.* [2001] we adopt air concentration of molecular chlorine in the lowest model layer over the ocean to be 100 ppt at nighttime and 10 ppt during the day and zero concentration over land. Besides, for the aqueous-phase chemistry cloud water was characterized by *pH* equal to 3.5 and water content of chloride ion $[Cl^-]$ as much as $7 \cdot 10^{-5}$ mole/L [*Acker et al.*, 1998].

To estimate the sensitivity of modeling results to chlorine concentration two additional model runs were performed with Cl_2 concentration value an order of magnitude lower (10 pptv) and higher (1 ppbv). The results show that, though, 10 times decrease of the Cl_2 concentration leads up to 80% decrease of oxidized gaseous mercury Hg^{2+} over the oceans, changes of total gaseous mercury (TGM) do not exceed 5% and the decrease of annual mercury deposition flux achieves the value of 25% only in the northern parts of the Atlantic and the Pacific. As to the regions of concern, changes of mean annual TGM and deposition flux are considerably lower in this area. Increase of Cl_2 concentration by an order of magnitude result in more significant changes: oxidized gaseous mercury Hg^{2+} increases several times in some marine regions, whereas mean annual TGM decreases by about 20% (mostly in the North Atlantic and the Pacific again). Annual deposition flux increases up to twice in these regions. However, changes of both mean annual TGM and deposition flux in the High Arctic and regions of the Russian North do not exceed 10%.

The model chemical scheme sensitivity to the value of chloride ion content in cloud water was investigated in [*Ryaboshapko et al*., 2001]. It was shown that the chemical scheme is sensitive only to very low values of chloride ion content (about $1 \cdot 10^{-6}$ mole/L). Additional calculation run with the chloride ion content $1 \cdot 10^{-6}$ mole/L showed that maximum changes of TGM concentration of about 5% are over industrial regions. Appropriate changes of total annual *Hg* deposition reaches 40% in those regions but do not exceed 15% in the Arctic.

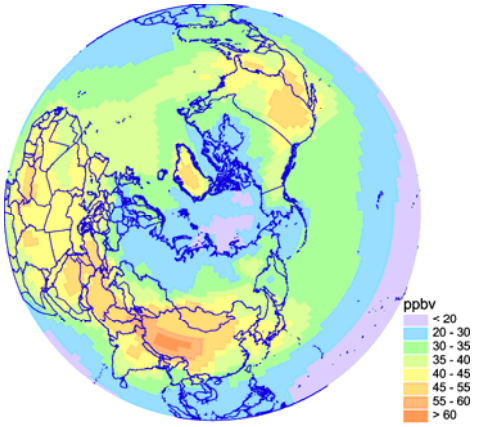

Figure 3.11. *Spatial distribution of ozone concentration in the ground air of the Northern Hemisphere*

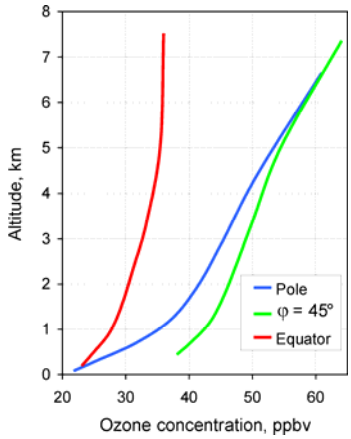

Figure 3.12. *Vertical profiles of ozone concentration averaged along different latitudes of the Northern Hemisphere*

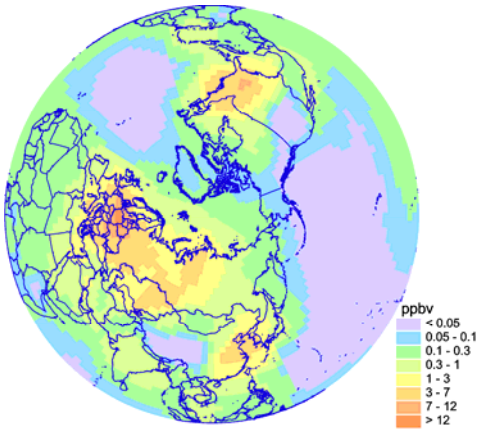

Figure 3.13. *Spatial distribution of SO_2 concentration in the ground air of the Northern Hemisphere*

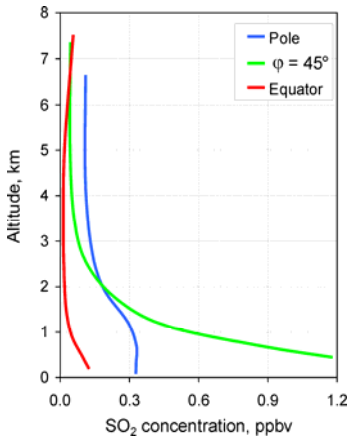

Figure 3.14. *Vertical profiles of SO_2 concentration averaged along different latitudes of the Northern Hemisphere*

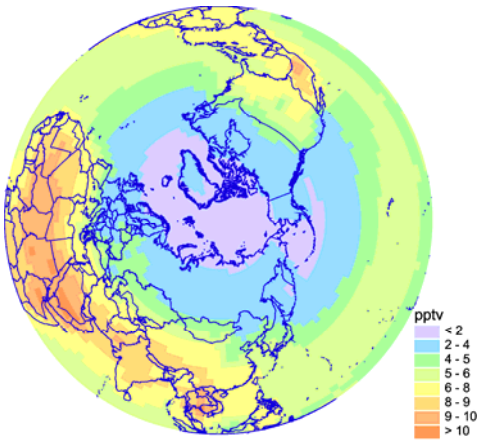

Figure 3.15. *Spatial distribution of HO_2 radical concentration in the ground air of the Northern Hemisphere*

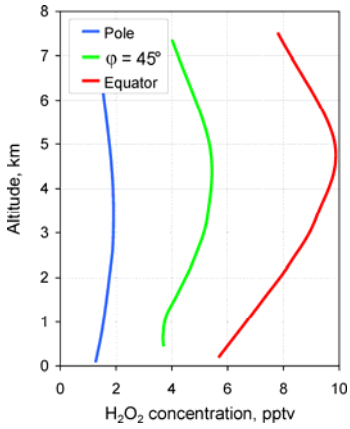

Figure 3.16. *Vertical profiles of HO_2 radical concentration averaged along different latitudes of the Northern Hemisphere*

3.8. Data on sea currents

The combined hemispheric model of the pollutants transport and diffusion, being developed under this project, consist of two main parts: atmospheric and oceanic. To determine the oceanic fields necessary for the transport-diffusion calculation (ocean currents, sea water properties), an ocean general circulation model (OGCM) is being used. The OGCM, which has been developing since early 90s, is based on primitive equations written in spherical coordinates [*Resnyansky and Zelenko*, 1991; 1992; 1999]. The following text will be put to the report instead of the above phrase: The former OGCM version had the limitation - the artificial zonal wall at 80N was placed, so that a near-pole area was excluded from the computational domain. During the second stage of the project implementation the model computational code was generalized in a special way to enable the inclusion of a near pole region into the model domain. The generalization involved the special finite differencing for the near-pole grid points taking into account the singularity of the latitude-longitude coordinate system. The model grid and bathymetry was constructed basing on data from the electronic version WOA98 oceanographic atlas [*NOAA Atlas*, 1998] (Fig. 3.17).

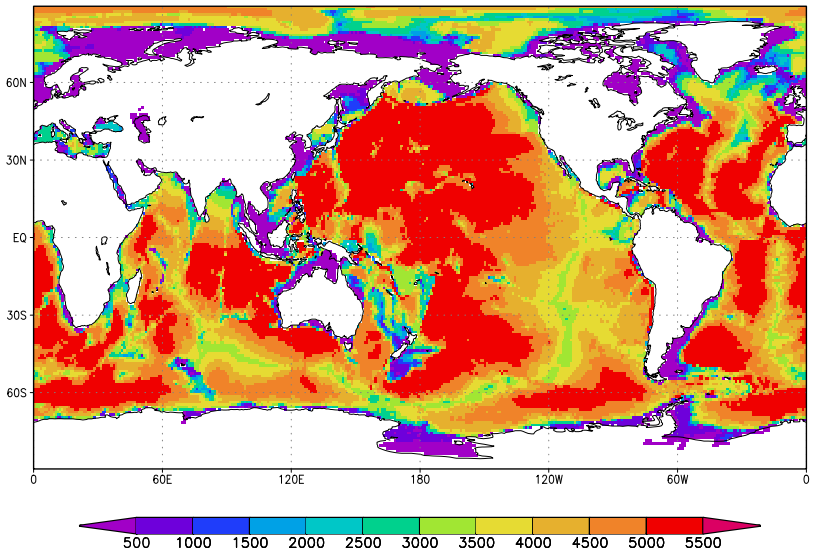

Figure 3.17. *The 1°x1° bathymetry (in meters) of the World Ocean used as input for the construction of OGCM computational domain*

The surface boundary conditions necessary to compute the evolution of oceanographic fields in OGCM are expressed in terms of atmospheric forcing: wind stress, heat and fresh water fluxes. This forcing, varying with time and horizontal space, has been determined from the NCAR/NCEP re-analysis data [*Kalnay et al.*, 1996].

One more modification of the OGCM involves the incorporation of observed data on sea surface temperature and ice cover distribution, which permits to improve the quality of the derived ocean characteristics.

A number of relatively short numerical experiments have been performed in order to tune the OGCM parameters. Figure 3.18 shows the integral transport stream function obtained after a two-month model integration in the global domain including the Arctic basin. As it is seen, the modified OGCM

version quite successfully simulates basic circulation elements of the Arctic basin [*Holland et al.*, 1996; *Zhang et al.*, 1998] – the transpolar water movement from the Chukot Peninsula to the Fram Strait, the cyclonic gyre northward of Severnaya Zemlya, the anticyclonic circulation in the Bofourt Sea.

The final configuration of the OGCM has been formed for a global domain with a horizontal resolution 1.25°×1.25° and with 15 levels in the vertical direction. Mean daily three-dimensional fields of ocean currents velocity and two-dimensional fields of the mixed layer depth were calculated for the further usage in hemispheric MSCE-POP transport model.

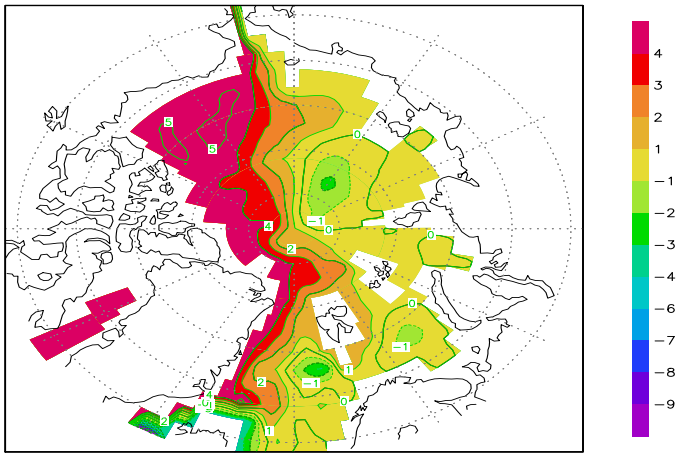

Figure 3.18. *Transport stream function in the Arctic basin. The water moves in such a way that higher function values are at right hand side of the observer moving with water. Values are in Sverdrups (1 Sv = 10^6 m^3/s)*

To illustrate obtained results several examples of obtained data on sea currents are given below. The Atlantic water mass of the Arctic basin, as it follows from the name, comes into the Arctic basin from the Atlantic Ocean initially as a surface inflow – the extension of Norwegian current, West Spitsbergen current and then submerges under the Arctic surface water. Several places where the surface flow submerges to deeper layers are known. One of them indicated on the majority of three-dimensional circulation schemes is located to the west of Spitsbergen Island. This submerging is reproduced in the ocean general circulation model used for the contaminants transport simulations. Figure 3.19 presents the distributions of the meridional current velocity component within two zonal sections across the Fram strait. It is clearly seen that the northward current detected in the latitude 76.25°N in the surface layer off the western coast of Spitsbergen Island is transformed into the flow submerging within the layer from 500 to 2500 m in the latitude 80°N. This pattern of abrupt submerging is typical of other places of inflow of the Atlantic water under the Arctic surface water.

The Pacific Ocean is another source of water inflow to the Arctic Basin through the Bering Strait. The mean inflow transport is about 0.8 Sv (1 Sv = 10^6 m^3/s.) [*Coachman and Aagaard,* 1988]. This average transport is superimposed by seasonal and interannual variations with amplitude of an order 1 Sv and 0.2 Sv respectively. According to [*Coachman,* 1993] they can reach 3 Sv to the north and 5 Sv to the south.

These features of temporal variability of the water exchange through Bering Strait are fairly well reproduced (Fig.3.20.a) by the ocean general circulation model. Similar variability occurs in other passages, through which the Arctic Ocean communicates with neighboring basins, for instance in Fram strait (Fig.3.20.b).

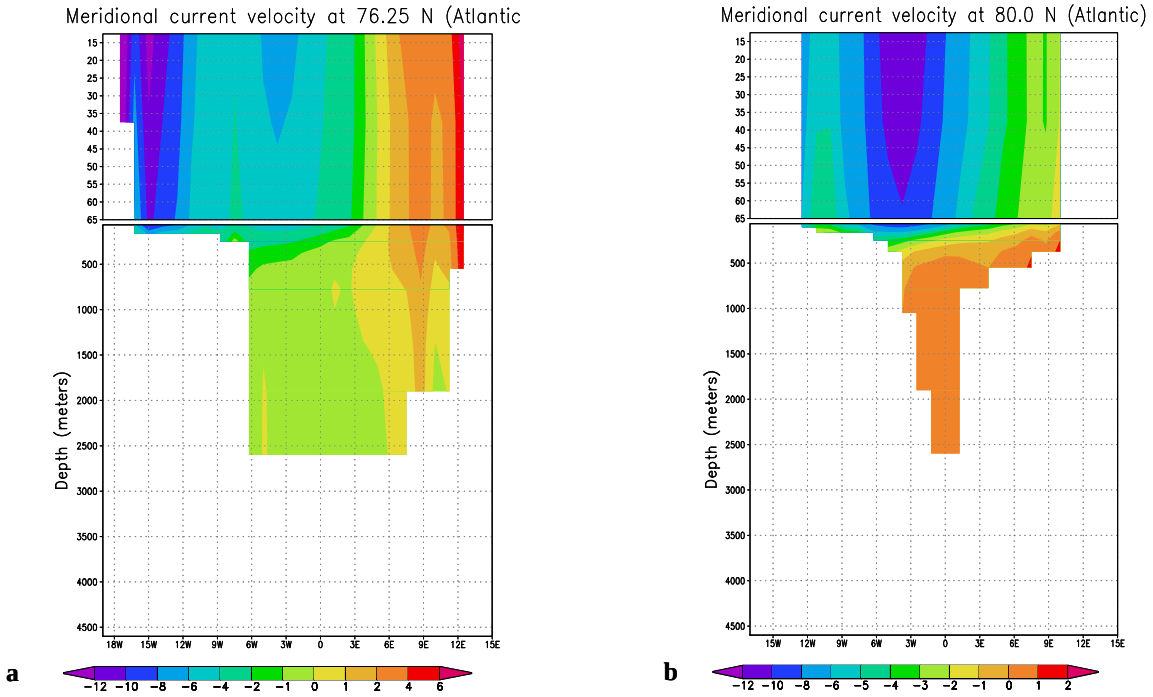

Figure 3.19 *The distribution of the meridional current velocity component (cm/s) within two zonal cross-sections through Fram strait along the latitudes 76.25° N (a) and 80°N (b). The velocity is averaged over the last (1997) year of the tree year ocean general circulation model integration on the 1.25°x1.25° grid within the computation domain involving the North Pole. Note: The velocity color scale is non-uniform: contour interval is 1 cm/s for velocities up to ±2 cm/s and 2 cm/s for velocities modules over 2 cm/s*

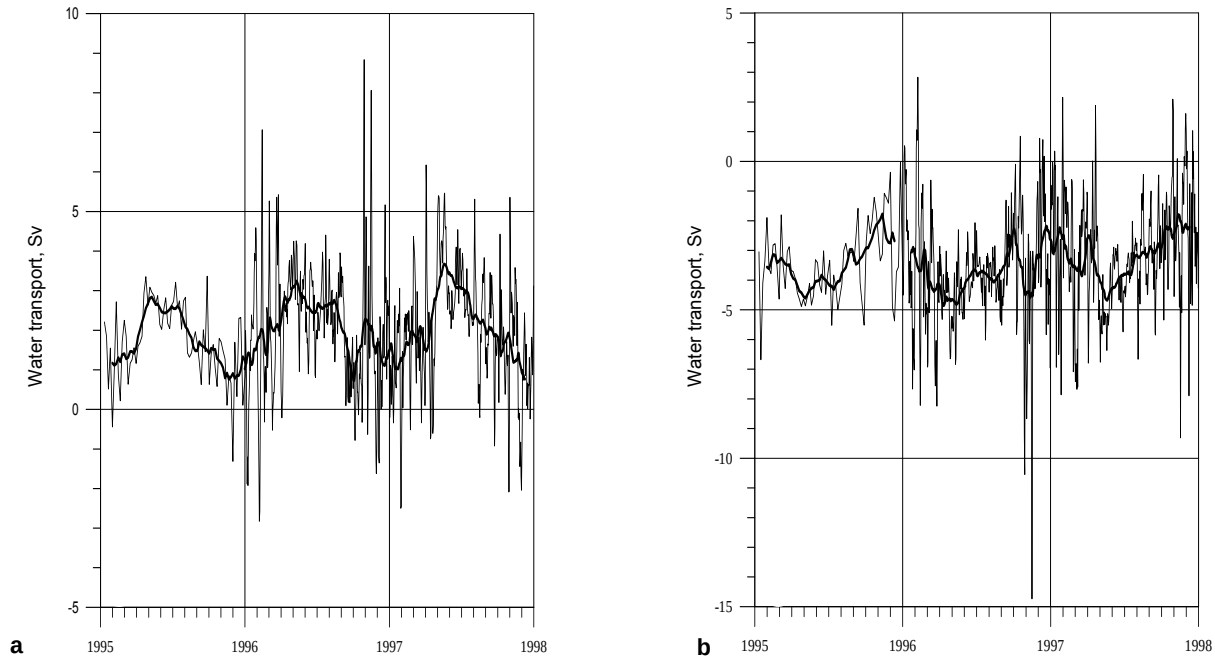

Figure 3.20 *Temporal variations of the overall transports through Bering strait (a) and Fram strait (b) over three years of 1.25°x1.25° grid model integration with daily atmospheric forcing derived from the NCEP/NCAR reanalysis. The flow transport is measured in Sverdrups (Sv, 1 Sv = 10^6 m^3/s). Positive values correspond to the northward water transport (from the Pacific to the Arctic Ocean In the Bering Strait and from the Atlantic to the Arctic Ocean in the Fram Strait). During 1995 the flow transport values are derived in each 5 days, during 1996-97- in a day. The bold line shows 45 days running mean*

3.9. Data on sea ice cover

The sea ice in polar regions is a mixture of open water, thin first-year ice, thicker multiyear ice, ice hummocks, snow at the top surface of ice, etc., i.e. presents non-uniform, non-isotropic medium. In this version of a simple model the sea ice is represented by three media: uniform ice, snow pack on the top of ice and open water. The evolution of the sea ice cover is governed by dynamic and thermodynamic processes. Current sea ice model includes the following processes:

- vertical heat fluxes between snow / ice and the atmosphere,
- vertical heat fluxes between ice and ocean,
- thermodynamic processes in polynyas,
- evolution of snow cover on the top of sea ice,
- ice cover dynamics in cavitational approximation,
- horizontal advection.

The heat balance equation at the upper ice surface (or snow if any) depends on heat flux due to evaporation from the surface (latent heat flux), sensible heat flux, downward long-wave radiation flux, downward short-wave (direct and scattered) solar radiation, surface albedo, and surface temperature.

The formation of new ice at the water surface in polynyas and marginal regions is determined by the net heat flux directed from the ocean to the atmosphere.

The snow pack dynamics involves precipitation, evaporation, melting and conversion of snow into ice.

The cavitational approximation in dynamics implies the resistance to compression (convergence), but absence of shear stress and resistance to divergence. In the dynamics equations there are terms of Coriolis forces, the stress induced by wind and sea currents, gravity forces arising due to sloping sea surface, and stress gradient due to ice compression.

The advection transport in the model affects all mass and thermodynamic parameters connected with sea ice.

Mean monthly output fields of the sea ice dynamics model, prepared as input data for sea ice POP transport model are

- ice thickness,
- ice compactness,
- ice / snow surface temperature,
- snow thickness on the top of ice,
- snow melting rate,
- ice melting rate at the upper boundary,
- ice melting rates at the lower and lateral boundaries.

Figure 3.21 demonstrates the simulated distribution of sea ice thickness and compactness for December and August. A large-scale structure of simulated fields is mainly consistent with distributions obtained from observations. The basic large-scale structure is well enough reproduced in

fields of ice thickness in winter and summer – the region of the most powerful perennial ice (Fig. 3.21 c,d).

Considering the obtained results as a whole it should be mentioned that model calculations make it possible to estimate characteristics of sea ice representing basic large-scale features of its evolution. In particular these data are applicable to the evaluation of impact on contaminants dispersion of such processes as ice screening impeding the exchange between the ocean and the atmosphere and comparatively long accumulation of contaminants in ice and their “rapid” discharge to the ocean during melting. To obtain more detailed and accurate data on ice cover evolution more comprehensive approach should be applied.

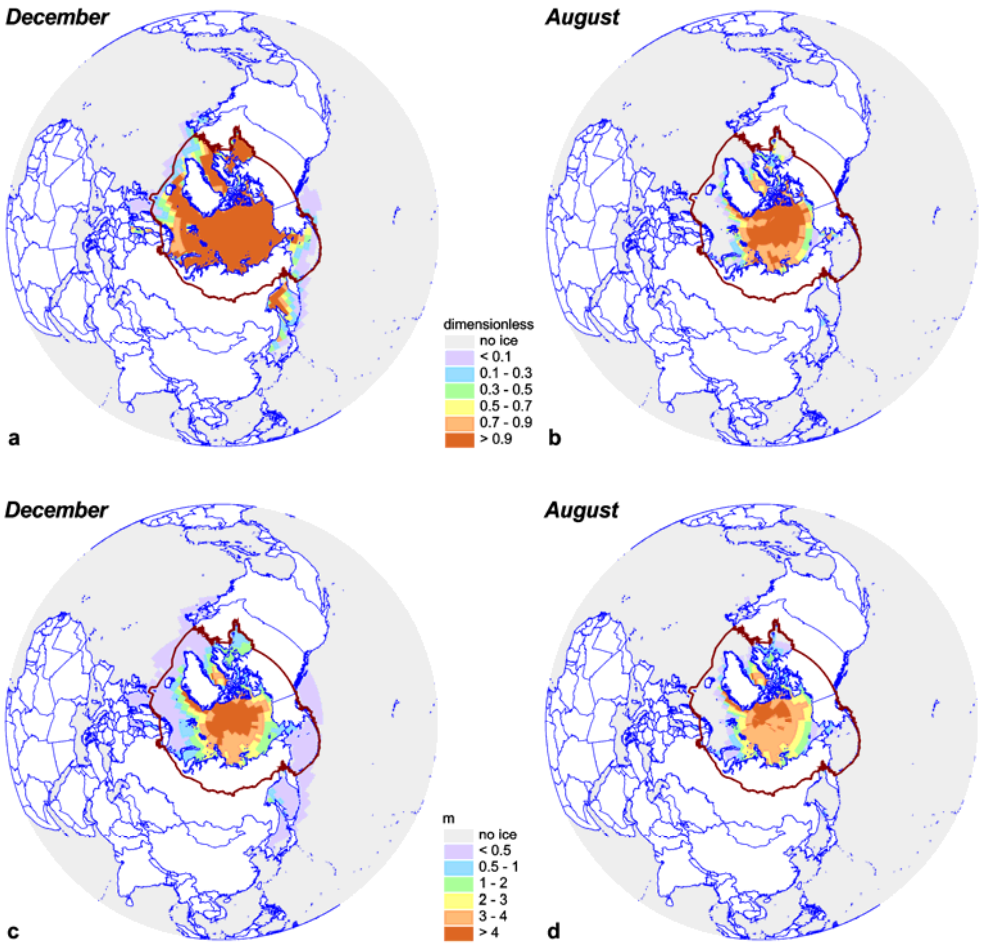

Figure 3.21. *Simulated distribution of ice compactness (a,b) and thickness (c, d) in December and August*

References

Acker K., D.Moller, W.Wieprecht, D.Kalass and R.Auel [1998] Investigations of ground-based clouds at the Mt. Brocken. Fresenius. *Anal. Chem.* v.361, pp.59-64.

Allen A.G., Nemitz E., Shi J.P., Harison R.M and Greenwood J.C. [2001]. Size distribution of trace metals in atmospheric aerosols in the United Kingdom. *Atmos. Environ*. , v.32, pp.4581 – 4591.

AMAP Assessment Report [1998] Arctic Pollution Issues, Arctic Monitoring and Assessment Programme, Oslo.

Banic C. M., W. H. Schroeder and A. Steffen [1999] Vertical distribution of total gaseous mercury in Canada. Book of abstracts, 5th International Conference on Mercury as a Global Pollutant, 23-28 May 1999, Rio de Janeiro.

Barrie L. A., Y. Yi, U. Lohmann, W.R.Leaitch, P. Kasibhatla, G.-J. Roelofs, J. Wilson, F. McGovern, C. Benkovitz, M.A. Meliere, K. Law, J. Prospero, M. Kritz, D.Bergmann, C. Bridgeman, M. Chin, J. Christensen, R. Easter, J. Feichter, A. Jeuken, E. Kjellstrom, D. Koch, C. Land and P. Rasch [2001]. A comparison of large scale atmospheric sulphate aerosol models (cosam): overview and highlights. Tellus v. 53, No.B, pp. 615-645.

Bergan T. and H. Rodhe [2001] Oxidation of elemental mercury in the atmosphere; constraints imposed by global scale modelling. *J. Atm. Chem.* v. 40, pp.191-212.

Bott A. [1989a] A positive definite advection scheme obtained by nonlinear renormalization of the advective fluxes. *Monthly Weather Review,* v.117, pp. 1006-1015.

Bott A. [1989b] Reply to comment on "A positive definite advection scheme obtained by nonlinear renormalization of the advective fluxes." *Monthly Weather Review,* v. 117, pp.2633-2636.

Chin M. et al. [1996] A global three-dimensional model of tropospheric sulfate, *J. Geophys. Res.* v.101, pp.18667-18690.

Christensen J. H. [1999]. An overview of Modelling the Arctic mass budget of metals and sulphur: Emphasis on source apportionment of atmospheric burden and deposition. Modelling and sources: A workshop on Techniques and associated uncertainties in quantifying the origin and long-range transport of contaminants to the Arctic. Report and extended abstracts of the workshop. AMAP report 99:4.

Christensen J.H. [1997] The Danish Eulerian Hemispheric Model - a three-dimensional air pollution model used for the Arctic. *Atmospheric environment*, v.31, No.24, pp.4169 – 4191.

Coachman L.K. [1993] On the flow field in the Chirikov Basin. *Cont. Shelf Res.*, v. 13, pp. 481-508.

Coachman L.K. and K. Aagaard [1988] Transports through Bering Strait: Annual and inter-annual variability. *J. Geophys. Res.*, v. 93, No C12, pp. 15535-15539.

Dabdub D. and J.H. Seinfeld [1994] Numerical advective schemes used in air quality models – sequential and parallel implementation. *Atmos. Environ.* v.28, pp.3369-3385.

Duyzer J.H., van Oss R.F., Verhagen H.L.M., Vervaart M. and B.Boekee [1997] Determination of deposition parameters of a number of persistence organic pollutantes by laboratory experiments. TNO-report TNO-MEP-R97/150.

Easter R. C. [1993] Two modified versions of Bott's positive-definite numerical advection scheme. *Monthly Weather Review,* v.121, pp.297-304.

Ebinghaus R., C. Temme, H.H.Kock, A. Löwe and W.H.Schroeder [2001] Depletion of atmospheric mercury concentrations in the Antarctic. Book of Abstracts, 6th International Conference on Mercury as a Global Pollutant, 15-19 October 2001, Minamata, Japan.

Ebinghaus R., R.M. Tripathi, D.Walischlager and S.E.Lindberg [1999] Natural and anthropogenic mercury sources and their impact on the air-surface exchange of mercury on regional and global scales. In: Ebinghaus R., Turner R. R., Lacerda de L. D., Vasiliev O., and Salomons W. (Eds.) Mercury contaminated sites. Springer, Berlin, 3-50.

Erickson D.J., III, C. Seuzaret, W.C. Keene, and S.L. Gong [1999] A general circulation model based calculation of HCl and $ClNO_2$ production from sea salt dechlorination: Reactive Chlorine Emissions Inventory. *J. Geophys. Res., v.* 104, No.D7, pp.8347-8372

Frolov A., A.Vaznik, E.Astahova, J.Alferov, D.Kiktev, I.Rosinkina and K.Rubinstein [1997a] A System of diagnosis of lower atmosphere for monitoring transboundary pollutant transport. *Meteorology and Hydrology*, No 4, pp.5-15.

Frolov A., A.Vaznik, E.Astahova, J.Alferov, D.Kiktev, I.Rosinkina and K.Rubinstein [1997b] A System of diagnosis of lower atmosphere for monitoring transboundary pollutant transport. The main algorithms. *Meteorology and Hydrology*, No 5, pp.5-13.

Frolov A., A.Vaznik, E.Astahova, J.Alferov, D.Kiktev, I.Rosinkina and K.Rubinstein [1997c] A System of diagnosis of lower atmosphere for monitoring transboundary pollutant transport: Precipitation and clouds. *Meteorology and Hydrology*, No.6, pp.5-15.

Frolov A., K.Rubinstein, I.Rosinkina, A.Vajnik, D.Kiktev, E.Astachova and J.Alferov [1994] A System of diagnosis of lower atmosphere for of transboundary air pollutant transport. EMEP/MSC-E and RHMC report 1/94.

Grell G.A., J Dudhia and D.R.Stauffer, [1995] A Description of the Fifth-Generation Penn State/NCAR Mesoscale Model (MM5). NCAR/TN-398+STR. NCAR Technical Note. June 1995. Mesoscale and Microscale Meteorology Division. National Center for Atmospheric Research, Boulder, Colorado, pp.122.

Guo, Y.-R., and S. Chen [1994] Terrain and land use for the fifth-generation Penn State/NCAR mesoscale modelling system (MM5): Program TERRAIN. NCAR Tech. Note, NCAR/TN-397+IA, 119 pp. [Available from the National Center for Atmospheric Research, P. O. Box 3000, Boulder, CO 80307.]

Gustin M. S., S.Lindberg, F.Marsik, A.Casimir, R.Ebinghaus, G.Edwards, C.Hubble-Fitzgerald, R.Kemp, H.Kock, T.Leonard, J.London, M.Majewski, C.Montecinos, J.Owens, M.Pilote, L.Poissant, P.Rasmussen, F.Schaedlich, D.Schneeberger, W.Schroeder, J.Sommar, R.Turner, A.Vette, D.Wallschlaeger, Z.Xiao and H. Zhang H. [1999] Nevada STORMS project: Measurement of mercury emissions from naturally enriched surfaces. *J. Geophys. Res*. v.104, No D17, pp. 21831-21844.

Hall B. [1995] The gas phase oxidation of mercury by ozone. *WASP* 80, pp.301-315.

Holland D.M., L.A.Mysak, J.M.Oberhuber [1996] Simulation of the mixed-layer circulation in the Arctic Ocean. – J. Geophys. Res., 101, №C1, p.1111-1128.

Hongisto M. [1998] HILATAR, a regional scale grid model for the transport of sulphur and nitrogen compounds. FMI Contributions No. 21, Finnish Meteorological Institute, Helsinki, Finland.

Iversen T., J.Saltbones, H.Sandnes, A.Eliassen and O.Hov [1989] Airborne tronsboundary transport of sulphur and nitrogen over Europe - model descriptions and calculations. EMEP/MSC-W Report 2/89, Meteorological Synthesizing Centre - West, Oslo, Norway.

Jackson T. A. [1997] Long-range atmospheric transport of mercury to ecosystems, and the importance of anthropogenic emissions - a critical review and evaluation of the published evidence. *Environ. Rev.* v.5, pp. 99-120.

Jacobs C.M.J. and W.A.J. van Pul [1996] Long-range atmospheric transport of persistent organic pollutants, I: Description of surface - atmosphere exchange modules and Implementation in EUROS. National institute of public health and the environment, Bilthoven, the Netherlands. Report No722401013.

Jacobson M. Z. [1999] *Fundamentals of atmospheric modeling*. Cambridge University Press. 656 p.

Jonsen J.E. and E. Berge [1995] Some preliminary results on transport and deposition of nitrogen components by use of Multilayer Eulerian Model. EMEP/MSC-W Report 4/95, Meteorological Synthesizing Centre – West, Oslo, Norway.

Junge C.E. [1977] Basic considerations about trace constituent in the atmosphere is related to the fate of global pollutant. In: Fate of pollutants in the air and water environment. Part I, I.H. Suffet (ed.) (Advanced in *Environ. Sci. Technol.,* v.8), Wiley-Interscience, New York.

Kalnay E., M. Kanamitsu, R. Kistler, W. Collins, D. Deaven, L. Gandin, M. Iredell, S. Saha, G. White, J. Woollen, Y. Zhu, A. Leetmaa, R. Reynolds, M. Chelliah, W. Ebisuzaki, W.Higgins, J. Janowiak, K. C. Mo, C. Ropelewski, J. Wang, Roy Jenne, Dennis Joseph [1996] The NCEP/NCAR 40-Year Reanalysis Project. - Bulletin of the American Meteorological Society, v. 77, No 3, p.437-471.

Keene W.C., M. Aslam, K. Khalil, D.J. Erickson, III , A. McCulloch, T.E. Graedel, J.M. Lobert, M.L. Aucott, S.L. Gong, D.B. Harper, G. Kleiman, P. Midgley, R.M. Moore, C. Seuzaret, W.T. Sturges, C.M. Benkovitz, V. Koropalov, L.A. Barrie, and Y.F. Li [1999] Composite global emissions of reactive chlorine from anthropogenic and natural sources: Reactive Chlorine Emissions Inventory. *J. Geophys. Res.* v.104, No.D7, pp.8429-8440.

Kiehl J.T. and B.P. Brieglep [1993] The relative roles of sulfate aerosols and greenhouse gases in climate forcing. *Science,* v. 260, pp.311 – 314.

Kim J. P. and W.F.Fitzgerald [1986] Sea-air partitioning of mercury in the Equatorial Pacific Ocean. *Science,* v.231, pp.1131-1133.

Koziol A.S. and J.A. Pudykiewicz [2001] Global-scale environmental transport of persistent organic pollutant. *Chemosphere*, v.45, pp.1181-1200.

Lammel G., J.Feichter and A.Leip [2001] Long-range transport and multimedia partitioning of semivolatile organic compounds: a case study on two modern agrochemicals. Report No.324.

Lin C.-J. and S.O.Pehkonen [1999] The chemistry of atmospheric mercury: a review. *Atmos. Environ.* v.33, pp.2067-2079.

Lin C.-J., M.-D. Cheng and W. Schroeder [2001] Transport patterns and potential sources of total gaseous mercury measured in Canadian high Arctic in 1995. *Atmospheric Environment*., v.35, pp.1141-1154.

Lindfors V., S.M.Joffre and J.Damski [1991] Determination of the wet and dry deposition of sulphur and nitrogen compounds over the Baltic sea using actual meteorological data. Finnish Meteorological Institute Contributions N 4, Helsinki.

Lurie Yu. Yu. [1971] *Handbook for Analytical Chemistry*. Khimiya, Moscow, 454 p.

Lyon B., G. Rice, O.R.Bullock and P.Selby [1999] Modelling the local scale atmospheric fate of anthropogenic mercury emissions. In: Mercury as a Global Pollutant. 5th International Conference, Rio de Janeiro, May 23-28, 1999. Book of abstracts, p. 110.

Marchuk G. I. [1975] *Methods of numerical mathematics*. Springer-Verlag, New York. 316 p.

Milford J.B. and Davidson C.I. [1985] The sizes of particulate trace elements in the atmosphere - A review. *JAPCA, v.* 35, No.12, pp.1249-1260

Mclachlan M. and M.Horstmann [1998] Forests as filters of airborne organic pollutants: a model. *Environ. Sci. Techno*l., v.32, pp. 413-420.

McRae G.J., W.R. Goodin and J.H. Seifeld [1982] Numerical solution of the atmospheric diffusion equation for chemically reacting flows. *Journal of Computational Physics,* v.45, pp.1-42.

NOAA Atlas [1998] NOAA Atlas NESDIS No. 27-32. U.S. Gov. Printing Office, Wash., D.C.

Odman M. T. and A.G. Russell [2000] Mass conservative coupling of non-hydrostatic meteorological models with air quality models. In: Gryning S.-E. and Batchvarova E. (Eds.) Air pollution modelling and its application XIII. Kluwer Academic/Plenum Publishers, New York, pp. 651-660.

Pacyna J.M. [1996] Emission inventories of atmospheric mercury from anthropogenic sources. In: Global and Regional Mercury Cycles: Sources, Fluxes and Mass Balances. Ed. By W.Baeyens, R.Ebinghaus and O.Vasiliev. NATO ASI Series, 2. Environment, v. 21. Kluwer Academic Publ., Dordrecht, pp. 161-177.

Pacyna, E. G. and Pacyna J. M. [2002] Global emission of mercury from anthropogenic sources in 1995. *WASP.* v.137, No. 1, pp.149-165.

Pankow J.F. [1987] Review and comparative analysis of the theories on partitioning between the gas and aerosol particulate phases in the atmosphere. *Atmos. Environ.*, v.21, pp.2275-2283.

Pekar M. [1996] Regional models LPMOD and ASIMD. Algorithms, parametrization and results of application to Pb and Cd in Europe scale for 1990 MSC-E Report 9/96, September.

Pekar M., A.Gusev, N.Pavlova, B.Strukov, L.Erdman, I.Ilyin and S.Dutchak [1998] Long-range transport of selected POPs. Development of transport models for lindane, polychlorinated biphenyls, benzo[a]pyrene. EMEP/MSC-E Report 2/98, Parts I.

Pekar M., N.Pavlova, A.Gusev, V.Shatalov, N.Vulikh, D.Ioannisian, S.Dutchak, T.Berg and A.-G. Hjellbrekke [1999] Long-range transport of selected persistent organic pollutants. Development of transport models for polychlorinated biphenyls, benzo[a]pyrene, dioxins/furans and lindane Joint report of EMEP Centres: MSC-E and CCC, EMEP Report 4/99.

Petersen G., A.Iverfeldt and J. Munthe [1995] Atmospheric mercury species over central and northern Europe. Model calculations and comparison with observations from the nordic air and precipitation network for 1987 and 1988. *Atmos. Environ*. v.29, pp.47-67.

Petersen G., J.Munthe, K. Pleijel, R. Bloxam and A.V.Kumar [1998] A comprehensive Eulerian modelling framework for airborne mercury species: Development and testing of the tropospheric chemistry module (TCM). *Atmospheric Environment*., v. 32, No. 5, pp. 829-843.

Pfirman S.L., H.Eicken, D.Bauch and W.F. Weeks [1995] The potential transport of pollutants by Arctic sea ice. *Science of the Total Environment* (NLD), v.159, pp.129-146.

Resnyansky Yu.D. and A.A.Zelenko [1991] Parametrization of the upper mixed layer in an ocean general circulation model. - Izvestiya of the USSR Academy of Sciences. *Atmosphere and Ocean Physics*, v.27, No 10, pp.1080-1088.

Resnyansky Yu.D. and A.A.Zelenko [1992] Numerical realization of the ocean general circulation with parametrization of the upper mixed layer. Proceedings of the USSR Hydrometcentre, v.323, pp.3-31.

Resnyansky Yu.D. and A.A.Zelenko [1999] Effects of synoptic variations of atmospheric forcing in an ocean general circulation model: direct and indirect manifestation. Meteorology and Hydrology, No.9 pp.66-77.

Rubinstein K. and D.Kiktev [1998] Comparison System of the Atmospheric Lower-Layer Diagnostic System(SDA) for Pollution Transfer Modeling of MSC - East(Moscow) and MSC - West(Oslo). Proceeding of International Conference of Air Pollution Modeling and Simulation. Paris, 26-29 October 1998.

Rubinstein K., Frolov A., Vaznik A., Astachova E., Rosinkina I., Kiktev D. and J.Alferov [1997] Diagnostic System of Atmosphere Lower-Layer for Pollution Transfer Modelling. Revista. International de Contaminational. Ambienal, v.13, No.1, pp.23-34.

Ruijgrok, W. Tieben H. and P.Eisinga [1997] The dry deposition of particles to a forest canopy: a comparison of model and experimental results. *Atmospheric Environment*, v.31, pp. 399-415.

Ryaboshapko A., I.Ilyin, A.Gusev, O.Afinogenova, T.Berg and A.-G. Hjellbrekke [1999] Monitoring and modelling of lead, cadmium and mercury transboundary transport in the atmosphere of Europe. Joint report of EMEP centres: MSC-E and CCC, EMEP Report 3/99, Meteorological Synthesizing Centre – East, Moscow, Russia.

Ryaboshapko A., Ilyin I., Bullock R., Ebinghaus R., Lohman K., Munthe J., Petersen G., Segneur C., Wangberg I. [2001] Intercomparison study of numerical models for long-range atmospheric transport of mercury. Stage I: Comparison of chemical modules for mercury transformations in a cloud/fog environment. EMEP/MSC-E Technical report 2/2001, Meteorological Synthesizing Centre – East, Moscow, Russia

Schryer D.R. (editor) [1982] Heterogeneous atmospheric chemistry. American Geophysical Union, Washington.

Sehmel G. A. [1980] Particle and gas dry deposition: a review. *Atmos. Environ.* v.14, pp. 983-1011.

Seigneur C., Karamchandani P., Lohman K., Vijayaraghavan K., and Shia R.-L. [2001] Multiscale modeling of the atmospheric fate and transport of mercury. *J. Geophys. Res*. v.106, No.D21, pp.27795-27809.

Sellers P.J., S.O. Los, C.J. Tucker, C.O. Justice, D.A. Dazlich, G.J. Collatz, and D.A. Randall [1994] A global 1 by 1 degree NDVI data set for climate studies. Part 2: The generation of global fields of terrestrial biophysical parameters from the NDVI. *International Journal of Remote Sensing*, v.15, No.17, pp.3519-3545.

Sellers P.J., S.O. Los, C.J. Tucker, C.O. Justice, D.A. Dazlich, G.J. Collatz, and D.A. Randall [1995]. A revised land surface parameterization (SiB2) for atmospheric GCMs. Part 2: The generation of global fields of terrestrial biophysical parameters from satellite data. Submitted to Journal of Climate.

Shatalov V., A.Malanichev, N.Vulykh, T.Berg and S.Manø [2001] Assessment of POP transport and accumulation in the environment. EMEP Report 4/2001, Moscow.

Slemr F. [1996] trends in atmospheric mercury concentrations over the Atlantic ocean and the Wank Summit, and the resulting concentrations on the budget of atmospheric mercury. In: Baeyens W., Ebinghaus R. Vasiliev O. (Eds.), Global and Regional Mercury Cycles: Sources, Flaxes and Mass Balances. NATO-ASI-Series, Kluwer Academic Publishers, Dordrecht, The Netherlands, pp. 33-84.

Spivakovsky C.M., J.A.Logan, S.A.Montzka, Y.J.Balkanski, M.Foreman-Fowler, D.B.A.Jones, L.W.Horowitz, A.C.Fusco, C.A.M.Brenninkmeijer, M.J.Prather, S.C.Wofsy, M.B.McElroy [2000] Three-dimensional climatological distribution of tropospheric OH: Update and evaluation, *J.Geophys.Res*., v.105, pp.8931-8980.

Strand A. and Ø.Hov [1996] A model strategy for the simulation of chlorinated hydrocarbon distributions in the global environment. *Water, Air and Soil Pollution,* v.86, pp.283-316.

Strukov B., Resnyansky Yu., Zelenko A., Gusev A. and V.Shatalov [2000] Modelling long-range transport and deposition of POPs in the European region with emphasis to sea currents. EMEP/MSC-E Report 5/2000.

Thomas G., Smith K.E.C., Sweetman A.J. and K.C.Jones [1998] Further studies on air-pasture transfer of polychlorinated biphenyls. *Environmental Pollution*, v.102, pp.119 - 128.

Travnikov O. [2001] Hemispheric model of airborne pollutant transport. EMEP/MSC-E Technical Note 8/2001, Meteorological Synthesizing Centre - East, Moscow, Russia.

Travnikov O. and Ryaboshapko A. [2002] Modelling of mercury hemispheric transport and depositions. EMEP/MSC-E Technical Report 6/2002, Meteorological Synthesizing Centre - East, Moscow, Russia.

Tsyro S. and L.Erdman [2000] Parametrization of aerosol deposition processes in EMEP MSC-E and MSC-W transport models. EMEP/MSC-W Technical Note.

US EPA [1997] Mercury Study Report to Congress. Vol. III, Fate and Transport of Mercury in the Environment. US-EPA-452/R-97003.

Vassilyeva G. and V. Shatalov [2002] Behaviour of persistent organic pollutants in soil. MSC-E Technical Note 1/2002.

Vulykh N. and Putilina V. [2000] Hexachlorobenzene: Properties, emissions and content in the environment. *EMEP/MSC-E Technical note 6/2000*, Meteorological Synthesizing Centre – East, Moscow, Russia.

Wang Y. J. et al. [1998] Global simulation of tropospheric O_3-NO_x-hydrocarbon chemistry 2: Model evaluation and global ozone budget. *J. Geophys. Res*. v.103, pp. 10727-10755.

Wania F. [1999] Global Modelling of Polychlorinated Biphenyls. June 1999.

Wania F. and D.Mackay [1999] Global Chemical Fate of α–Hexachlorocyclohexane. 2. Use of a Global Distribution Model for Mass Balancing, Source Apportionment, and Trend Prediction. Environmental Toxicology and Chemistry, v.18, No.7, pp.1400-1407.

Wania F., D.Mackay, M.McLachian, A.Sweetman and K.Jones [1999] Global Modelling of Polychlorinated Biphenyls. Synopsis of Research Conducted under the 1998/99 Northern Contaminants Program. Indian and Northern Affairs, Canada, pp.61-70.

Weiss R.E., Waggoner A.P., Charlson R.J., and Ahlquist N.C. [1977] Sulfate aerosol: its geographical extent in the mid-western and southern United States. *Science* v.195, pp.979 – 981.

Whitby K.T. [1978] The Physical Characteristics of Sulphur Aerosols. *Atmos. Environ.* , v.12, pp.135 – 159.

WMO [2000] Report and proceedings of the WMO/EMEP/UNEP workshop on modelling of atmospheric transport and deposition of persistent organic pollutants and heavy metals (Geneva, Switzerland, 16-19 November 1999).

Yanenko N. N. [1971] *The method of fractional steps. The solution of problems of mathematical physics in several variables*. Springer-Verlag, New York. 160 p.

Yu Lu and M.A.K. Khall [1991] Tropospheric OH: model calculation of spacial, temporal and secular variations. *Chemosphere*, v. 23, pp.397-444.

Zhang J., W.D.Hibler III, M.Steele and D.A.Rothrock [1998] Arctic ice-ocean modeling with and without climate restoring. *J. Phys. Oceanogr.*, v.28, No 2, pp.191-217.